

# Nanostructured gold layers. III. Functionalization of gold layers obliquely deposited onto polystyrene substrate

I. ZGURA, T. BEICA, S. FRUNZA, L. FRUNZA\*, C. COTIRLAN-SIMIONIUC, F. UNGUREANU, N. GHEORGHE, O. RASOGA, T. VELULA, C. ZAHARIA<sup>a</sup>

*National Institute of Materials Physics*

<sup>a</sup>*Institute of Virology St. S. Nicolau of the Romanian Academy*

Hexadecanethiol monolayers were self-assembled onto nanostructured gold layers (10-20 nm) deposited onto glass by using an intermediate polystyrene layers (50 nm). We found that these glass plates with an intermediate PS layer do not peel under overnight immersing in ethanol solution of hexadecanethiol. The thiol and gold layers were characterized by several methods such as X-ray diffraction, X-ray photoelectron spectroscopy, spectroellipsometry (SE) and Raman spectroscopy. The thickness of the thiol layer was estimated from SE measurements to be ca 1 nm, meaning less than the length of the molecule; it was then inferred that the molecule is tilted onto gold, as expected from the behavior of other self assembled monolayers (SAMs) obtained under similar conditions. It is noteworthy that the alignment of a nematic liquid crystal in a cell having the plates deposited with the hexadecanethiol SAMs is still uniform, despite the multilayer structure of the substrate on the glass plates.

(Received March 18, 2010; accepted August 12, 2010)

*Keywords:* Nanostructured gold layer, Polystyrene substrate, Alkanethiol SAM, Alignment of liquid crystals

## 1. Introduction

Recently it was shown that self-assembled monolayers (SAMs) can be formed from alkanethiols on the surface of gold, either as single crystals or as thin films [1-6] these monolayers can further specifically bind proteins. If these bonds are formed in the presence of aligned liquid crystal (LC) molecules, the alignment is disturbed and thus reports the presence of the proteins [5-11].

In the first paper of the series [12] we have established the experimental conditions for the deposition of nanostructured gold layers on the surface of glass plates by vaporization at small incidence angle (large angle with the normal direction) leading to nanostructured columnar semi-transparent layers. Then the layers were characterized by complementary methods; additional support was given by observing the molecular alignment present in the liquid crystal cells obtained with these gold layers.

However, the nanostructured gold layers obtained directly onto the glass support have a rather short life especially when they work in watery solutions. Instead of improving the gold adherence by deposition of certain substrates [13-15] which may lead to decreasing the optical transmission of the functionalized liquid crystal cells made with these deposited plates, we have used polystyrene (PS) layers [16] containing benzene rings that might interact with gold atoms [17]. A rather strong interaction of gold atoms with the substrate molecules was found indeed on the basis of the X-ray diffraction (XRD) and spectroellipsometry (SE) measurements [16].

In this paper the results obtained in functionalization of the nanostructured gold layers deposited onto a PS substrate by self-assembling of hexadecanethiol are presented. We found that functionalization with this long chain alkanethiol offers consistent alignment properties in a displaying cell with nematic liquid crystal.

## 2. Experimental

*Glass plates* of float soda-lime type were commercially available and cut at the size 32x23x3 mm. Before use these plates were very carefully cleaned [12].

*Polystyrene layers* were deposited onto glass plates by spin coating with a solution of atactic polystyrene 1.5 wt% in toluene, at 3000 rpm [18,19]. The plates were slowly dried in the laminar hood; afterwards they were heated at 100°C for ½ h.

*Gold vapor deposition* at oblique incidence was performed (onto the glass plates) with the Hochvakuum B30.2 equipment (Dresden, Germany) as previously described [12]. The thickness of the deposited layer was estimated by using oscillating quartz monitor. The deposition was performed onto an intermediate polystyrene (PS) film at angles resulted from the found nomograms. Details (the incidence angle of gold deposition  $\theta$  and the thickness  $T$  of the gold layer) are given in Table 1. Because adventitious adsorbates collect on the gold, the plates were kept under protective atmosphere and used further as quickly as possibly (ages measured from the time of removal from the evaporator were mostly under 2 h but till 2 weeks when intended).

Table 1. Parameters of the gold deposition.

Sample batch	$\theta$ /degree	$T^*$ /nm
P(1)	40	20
P(2)	80	12
P(3)	80	10
P(4)	60	10
P(6)	60	20

\*estimated from the quartz monitor indications.

Functionalization of the gold with alkanethiol was achieved by immersing the gold deposited glass plates in a solution 0.00246 wt% of hexadecanethiol (Aldrich) (here abbreviated  $C_{16}SH$ ) in absolute ethanol (Merck) for  $\sim 16$  h at room temperature. The glass plates were thus arranged inside the Petri vessels to prevent their overlapping; in addition, the vessels were kept sealed off to avoid solvent evaporation. After the period of the formation of the thiol layers, the plates were thoroughly rinsed with ethanol and dried under a stream of nitrogen gas. These plates were kept (in shadow) in a special box with dry atmosphere and further used as soon as possibly.

To characterize the structure and the thickness of the deposited layers, several methods were applied. Thus, X-ray diffraction (XRD) measurements were done with an equipment D8 Advance (Bruker-AXS) at a grazing incidence angle. The equipment for spectroellipsometric investigations was a DUV-VIS-XXNIR Variable Angle Spectroscopic Ellipsometer (Woollam); the spectral domain spreads between 193 and 2200 nm while three incidence angles ( $65^\circ$ ,  $70^\circ$ ,  $75^\circ$ ) were set to measure the ellipsometric angles  $\psi$  and  $\Delta$ . Cauchy model with optical constant variation was then applied to interpret the SE data. X-ray photoelectron spectroscopy (XPS) studies were done with an updated spectrophotometer VG ESCA MKII, with Al source ( $K_{\alpha}=1486.6$  eV), at a take-off angle of  $55^\circ$  [20], using SDP 32 and S-PROBE software. Peak positions were assigned by referencing the  $Au(4f_{7/2})$  peak to a binding energy of 83.95 eV and linearly shifting all other XPS peaks by an equal amount, as it is customary. Raman spectroscopy (RS) measurements were performed with a FT Raman Bruker RFS 100/S and a Jobin Yvon T64000 Raman spectrophotometer at excitation wavelengths of 1064 and 514 nm. Raman spectra were recorded at room temperature in a backscattering geometry with a resolution of  $4\text{ cm}^{-1}$ .

Liquid crystals symmetric cells with gold layer similarly deposited onto both cell plates and directed toward the cell inside were then obtained [12,16] from the deposited glass plates. The two glass plates were arranged so that the evaporation/deposition direction was anti-parallel (see Figure 1): Main evaporation direction and possible orientational directions of the LC molecules (A, B, H and P) are there shown. A, B and H are in the evaporation plane while P is perpendicular onto this plane. The cell thickness was  $15\mu\text{m}$  (by Mylar spacer). For all samples, the plates were held together, especially during the handling of the cells, at two opposed ends using binder bulldog clips. The liquid crystal was 4-*n*-pentyl-4'-

cyanobiphenyl (5CB) (Merck), having transition temperature  $35.4^\circ\text{C}$ . It was introduced into the cell in the isotropic state (at  $40^\circ\text{C}$ ) by capillary action. The cell was then cooled to room temperature. During the cooling process, 5CB changed from its isotropic state to its nematic state.

LC cells were optically examined under crossed polarizers by direct visualization or in transmission mode on a polarized light microscope (Leitz Orthoplan) with a digital camera (Panasonic DMC-FZ8). Consistent settings of both the microscope light source (numerical aperture 0.6) and the digital camera allowed for the direct comparison of images taken for different samples. In-plane birefringence was determined orthoscopically by rotating the stage by  $45^\circ$  and observing the extent of modulation in the intensity of transmitted light. Conoscopy technique (in a convergent light beam) was used to confirm the homeotropic alignment of the liquid crystal.

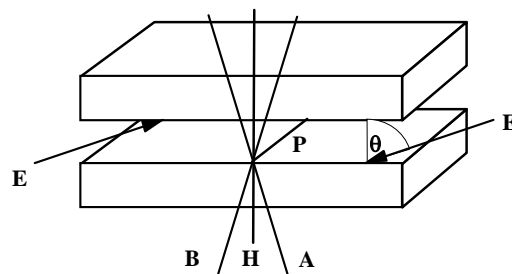


Fig. 1. Two (gold) deposited glass plates assembled in a liquid crystal cell. E is the main evaporation direction of the gold and A, B, H and P are the possible orientational directions of the LC molecules. E, A, B and H are in the evaporation plane while P is perpendicular onto this plane.

### 3. Results and discussion

The results were obtained in the bottom up technique and were presented as follows.

Polystyrene and gold layers were successively deposited onto glass support. Planar or respectively controlled topography deposition were thus realized and the layer features were found as described previously [12,16]. Obliquely deposited gold films were prepared by using a fixed angle of incidence of the metals and stationary substrates. The angle of incidence used in this study was  $40^\circ$ ,  $60^\circ$  or  $80^\circ$ , measured from the normal of the substrate. Gold nanoparticles have the face-centered cubic structure, most of them offer the face (111) as the lowest energy surface. PS layers have a thickness of ca. 50 nm while gold layers have a thickness of 10 or 20 nm and a columnar structure. A rather strong interaction between gold atoms and the polystyrene molecules in the substrate was put in evidence. These findings are not further discussed.

Hexadecanethiol layers were then self assembled onto the gold substrates. The formation of an initial lying-down

phase, the development of a standing-up phase and the structure of self assembled monolayers (SAMs) formed on Au(111) from solutions of long chain alkanethiols [ $\text{CH}_3(\text{CH}_2)_n\text{SH}$ ,  $n > 9$ ] has been extensively studied. As it was reviewed in (e.g. in Ref. [21]), sulfur atoms form a commensurate  $(\sqrt{3} \times \sqrt{3})R30^\circ$  structure with a nearest sulfur-sulfur spacing of 4.97 Å, while the alkyl chains also form a hexagonal lattices with a unit mesh constant of  $\sim 5$  Å, which is consistent with the structure of sulfur atoms. Some unit cells might contain more than one chain. The alkyl chains tilt by  $\sim 30^\circ$  from the surface normal and rotated around the chain axis by an angle (twist angle) of  $\sim 52^\circ$ , to maximize their van der Waals interactions. The formation of close-packed, crystalline-like monolayers with a nearly all-trans configuration was inferred. The chains on the Au(110) surface tilt more from the surface normal ( $\sim 37^\circ$ ) than on the Au(111) surface, while on Au(100), the interchain spacing is too small, to accommodate longer chains with an extended all-trans conformation: the packing is then more dense on Au(100) than on Au(111) and (110) surfaces. Therefore, in our case of the given chain length (of the alkanethiol) and of the applied preparing procedure we supposed that a self assembling process took place with a rather high degree of order [22].

The SAMs formed in our samples were characterized in the first part of this work, where the results obtained by X-ray photoelectron spectroscopy, spectroellipsometry and Raman spectroscopy measurements are presented.

The second part of the work describes the effect of the functionalization of the nanostructured gold layers (in our case particularly deposited onto PS substrate) on the LC alignment in a LC cell as followed up by simple visualization or by optical microscopy.

### 3.1. SAM formation onto nanostructured gold layers

#### 3.1.1. XPS studies

A representative survey spectrum is presented in Figure 2 together with the expected positions of the main lines. Such survey XP spectra either of a nanostructured gold layer on glass substrate or of a nanostructured gold layer on PS substrate, the latter after immersing overnight in a C16SH solution show only the peaks due to C, O, Au, S, namely those peaks of the expected elements. A common feature in these spectra is the presence of (carbon and) oxygen. The high-resolution elemental narrow scans

of C(1s), S(2p), Au(4f) and O(1s) regions on two samples containing SAMs onto nanostructured gold layers deposited over PS substrate are illustrated in Figure 3, together with their signal analysis.

Carbon peak of ca. 284.6 eV binding energy (BE) is the highest among the components of the C(1s) peaks. The signal analysis indicates also the presence of a lower intensity C(1s) states at 282.1 - 282.5 eV and 280.8 - 281.1 eV (Figure 2). The asymmetry toward higher BEs can be solved by introducing the forth C(1s) low intensity peak (not shown in Figure 2) toward 287 eV. The peak at ca. 284.6 corresponds mostly to carbon of thiol methylene groups but also to an adventitious carbon on surface both present in the substrates and due to atmospheric contamination; these contributions to the main signal thus explain its high intensity. The other C(1s) states appearing with lower intensity peaks at 282.1-282.5 eV and 280.8-281.1 eV, might be attributed at first glance to aromatic type carbon atoms belonging to the gold interfaces with the organic layers. To identify the carbon species bound to the surface, we remember that, in the organic molecules, the carbon atoms directly bound/close to oxygen atoms are shifted to a relatively high binding energy of 287.3 eV [23-26]; no such carbon seems to be present on our samples. Instead, methylene (from thiol, in our case) and benzene (e.g. from polystyrene) units were usually found at 284.2 eV and 284.7 eV, respectively [27]. Another interpretation of the carbon peaks at 282.1 - 282.5 eV and 280.8 - 281.1 eV might be related to the surface inhomogeneity and charging, while the additional peak at 287 eV (correlated to the B peak of the oxygen, see below) might be due to carbonyl groups by partial oxidation of the surface carbon atoms.

Oxygen is present in two (1s) states: one at ca. 531 eV binding energy and another one at lower BE value. One may suppose that the first peak is given by the surface oxygen and the second, by the oxygen at the interface gold-thiol.

The XPS data suggest that the major sulfur species present is a thiolate: the S(2p) core levels are shifted by over 1 eV to lower binding energy from the position expected for a thiol (with the S-H bond intact). The binding energies measured for the S(2p<sub>3/2</sub>) core level(s) on gold are all well within the range expected for the surface thiolate (RS-M or RS-M<sup>+</sup>) species [28,29]. The values would then implicate a dissociative adsorption of the S-H bond on the metal atoms of the substrate:



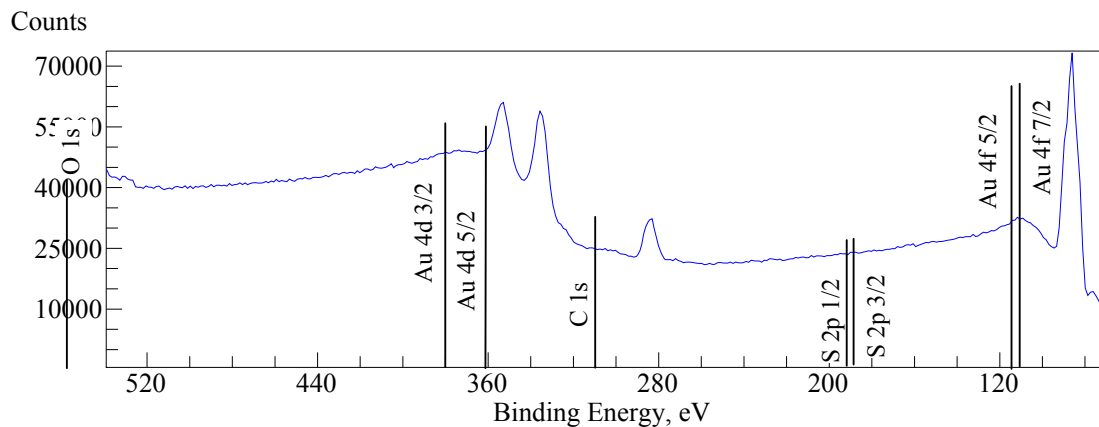


Fig. 2. Survey XPS spectrum of C16SH-P(3) sample in an extended abscissa; the vertical lines show the position of the most expected binding energies.

In fact, each S(2p) core level can be decomposed into two spin-orbit components of equal width (1.0 - 1.2 eV) whose integrated areas are in the ratio  $2J+1$  (i.e., 1:2;  $J = 1/2, 3/2$ ) [30,31]. These components are shown in Figure 3.

The XPS data also suggest that the bonding at the surface can be heterogeneous (a broad S(2p) envelope is seen). This heterogeneity cannot be attributable to different metal bonding sites since the Au(111) is prevalent [12,16], but is due to different sulfur valence states. Conveniently identifying the doublets with the energy of their  $2p_{3/2}$  component, the lower BE doublet ( $S_A$  species) occurs at  $\sim 162$  eV and the higher BE doublet ( $S_B$  species) is found at  $\sim 165$  eV. A sulfur signal at 162 eV has been reported in a numerous series of papers on organosulfur SAMs on gold and has been assigned to a thiolate species. Literature investigations (cited by Zhang [27]) allow inferring that if two such samples have different binding energies, they may have different coverages: This might be also the case of our samples. The assignment of the  $S_B$  species is less straightforward. Thus, S(2p) signals in the 163.2 - 163.6 BE range have been observed in pristine SAM samples and assigned to unbound molecules on poorly rinsed long chain alkanethiol SAMs or to second layer molecules hydrogen-bonded to the first layer molecules in short chain SAMs [32]: these are not met in our samples. Another possible assignment of the  $S_B$  species takes into account the occurrence of X-ray- or light-induced molecular damage [33]. We might also suppose that this peak is due to the degradation of the SAMs by formation of sulfonates or disulfide bridges: For a sulfur bound to oxygen, the peak position is at a BE higher than 166 eV [22,32,33]:

However, this bonding is not clearly seen in the oxygen states. Anyhow, the intensity of this latter peak is rather low and this fact introduces more uncertainty in discussing its attribution.

The adsorption of a thiol SAM on the gold surface does not seem to result in a significant perturbation of the Au(4f) core level spectrum determined by XPS: The intense and well shaped peaks were easily fitted. Moreover, the 4f spin-orbit splitting was ca. 3.7 eV in satisfactory agreement with other results [34,35] in the metallic gold. Careful examination of the spectra in Figure 2 shows that the full width at half-maximum are a little larger than in the absence of the SAM, especially for the sample C16SH-P(3). Besides, especially the core level Au(4f7/2) (referenced at 83.95 eV) has an asymmetric tail of the peak in the region toward the small BEs in the presence of the organic overlayer. Its presence can be explained knowing [36] that the formation of electron-hole pair in metals leads to a tail toward smaller kinetic energy (higher binding energy) due to the electron excitation from the valence band in the quasi continuum conduction band. No clear indication in the gold spectrum can be related to the gold-sulfur bonding under the given experimental conditions.

The acquired XP spectra allow calculating the atomic composition of the SAMs. Atomic concentrations were determined by numerical integration of the relative peak areas in the detailed element scans using the literature sensitivity factors [37,38]. Table 2 shows the atomic compositions thus derived. The absolute compositions derived from XPS should be interpreted with caution, since photoelectrons from the subsurface atoms are attenuated by the overlying material [31]. The

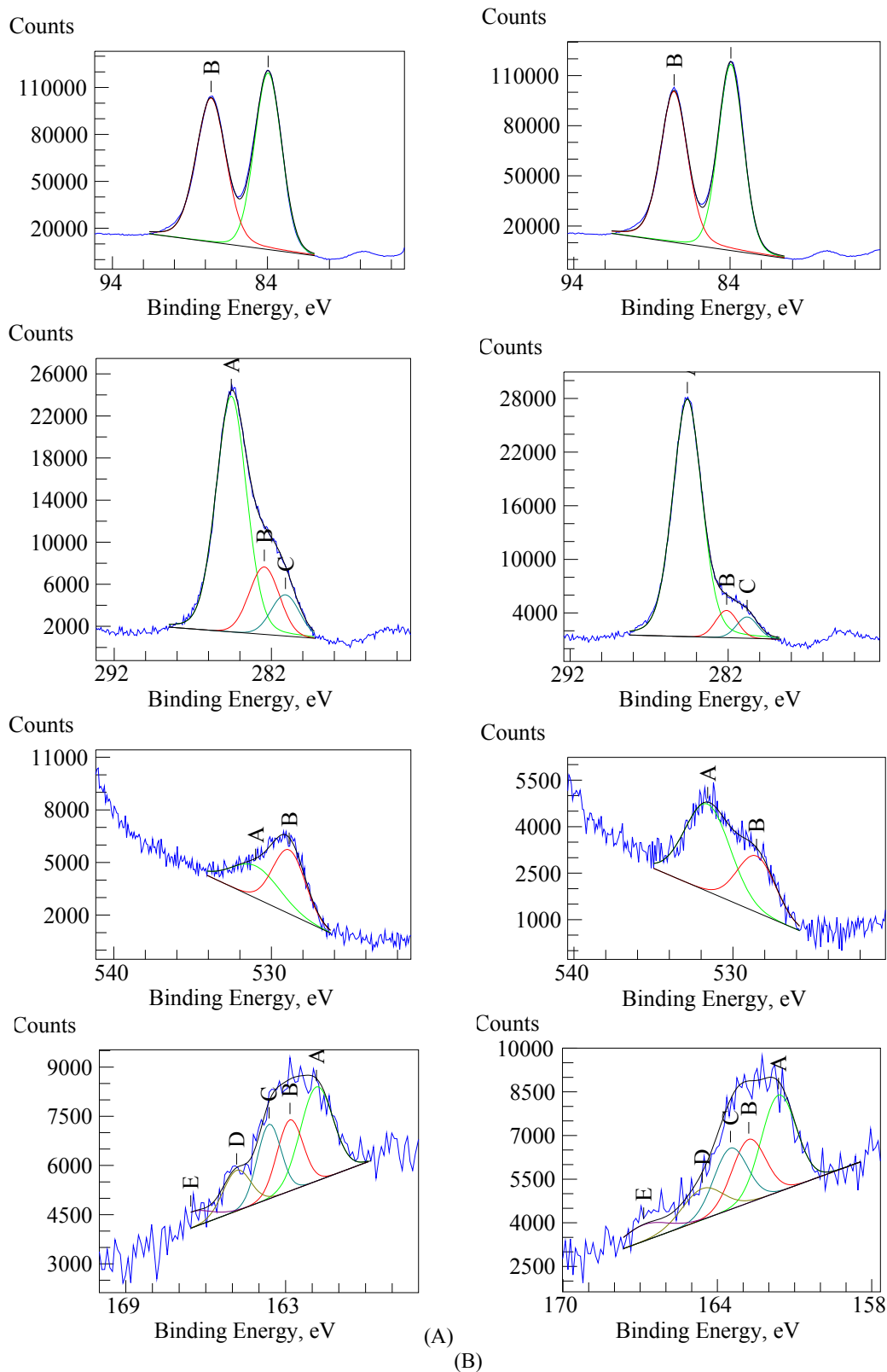


Fig. 3. High-resolution elemental XP spectra of (A) C16SH-P(3) sample; (B) C16SH-P(4) sample (viewed in colors in the online issue). The components and the best fit are overlapped on the data. From up to down the spectra belong to Au(4f), C(1s), O(1s) and S(2p) core level.

observed and calculated compositions agree reasonably well with each other, taking take-off angle, photoelectron attenuation, and possible variations in coverage into account

Table 2. Composition of the SAM layers.

Sample	Composition wt%			
	O	C	Au	S
C16SH-P(3)	2.9	74	22 (95.1)*	1.1 (4.9)*
C16SH-P(4)	4	72.3	21.7 (91.4)*	2 (8.6)*

\*composition of the thiol substrate.

Table 2 shows that sulfur exhibits higher atomic concentration in the SAM of the sample C16SH-P(4) than in the SAM of the sample C16SH-P(3).

### 3.1.2. SE studies

Ellipsometry is an invaluable technique for measuring film thickness of the (alkane)thiols adsorbed on gold [10,39-41].

The SE results are conventionally presented reporting the value of the  $\Delta$  and  $\Psi$  ellipsometric angles as a function of the wavelength [42].  $\Delta$  and  $\Psi$  are defined through the relation

$$\rho = R_p / R_s = \tan \Psi \exp(i\Delta)$$

where  $R_p$  and  $R_s$  are the complex reflection coefficients for s- and p-polarized light [37], respectively. The parameter  $\Delta$  carries most of the information on the overlayer thickness, while  $\Psi$  is mainly related to the near-surface gold electronic structure [43,44] and is affected by the organic overlayer to a lesser extent.

Representative SE spectra obtained at 70° of incidence on thiol-covered samples are shown in Figure 4 together with spectra collected on corresponding bare substrates. The data taken on a single sample were characterized by a good repeatability.

Fig. 4 indicates a change of  $\Delta$  after the layer deposition: firstly of Au, then of thiol. For a quantitative data analysis we simulated the spectra by using a Cauchy model, we obtained a layer thickness (Table 3) that, by comparison with the estimated length of the molecule in all trans methylene conformation (about 2.2 nm), can be interpreted as the formation of a molecular layer of possibly tilted molecules, with coverage less than 1.

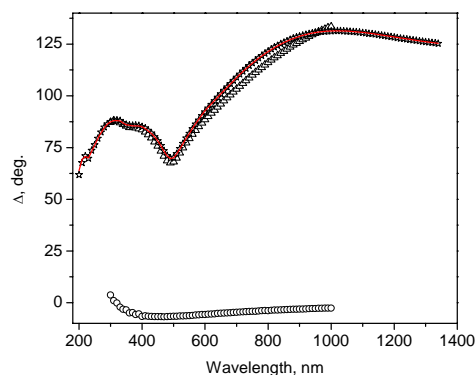
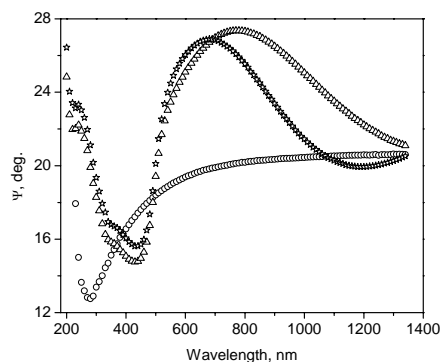


Fig. 4. Ellipsometric angles vs. wavelength for the sample P(4) in different steps of layer deposition as follows: empty circles – polystyrene, empty up triangles – Au, empty stars – C16SH. The solid line (viewed in red in the online issue) is the model fit. The incidence angle of the light was 70°.

The ellipsometric thicknesses of our SAMs indicate a SAM layer thicker on sample C16SH-P(4) than on C16SH-P(3) in agreement with the XPS measurements. At the same time, this thickness is a little less than that found by Shah et al. [45] for their SAMs of hexadecanethiol.

Table 3. Layer thickness (in nm) from SE data

Layer\Sample	C16SH-P(3)	C16SH-P(4)
Polystyrene	51.3	51.0
Gold	7.3	9.1
SAM	0.8	1.2

### 3.1.3. Raman spectroscopy studies

The importance of RS measurements comes from the obtaining of the vibrational spectrum, which displays fingerprinting information of the chemical composition of the layers. The layers onto our samples were suitable to be studied by RS because of the presence of the metal surface's roughness features, which increase the signal, and of the changes in the adsorbate electronic states due to chemisorption of the analyte. In fact we expected a selectivity of surface signal resulting from the presence of surface enhancement mechanisms [46].

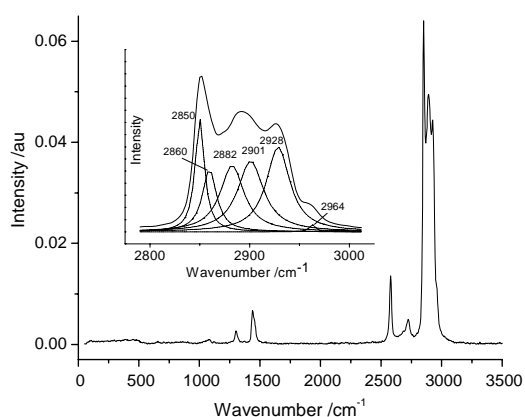


Fig. 5. Raman spectrum of C16SH in solid state recorded with  $\lambda_{exc} = 1064$  nm. The inset enlarges the CH stretching region and gives a possible decomposition into Gaussians.

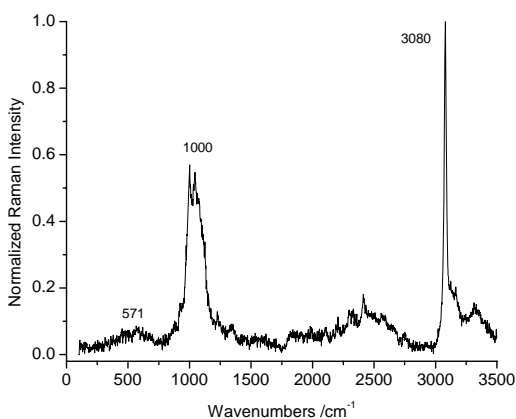


Fig. 6. SERS spectrum of the SAM deposited onto Au substrate (sample C16SH-P(1)) Spectrum is recorded with  $\lambda_{exc} = 514$  nm.

Fig. 5 presents the Raman spectrum obtained for hexadecanethiol in solid state. The most important expected peaks are present. A possible deconvolution in the region 2800–3000  $\text{cm}^{-1}$  into Gaussian components is shown in the same figure. Unfortunately, large and broad fluorescence present in the spectra (at the same excitation wavelength) of the samples corresponding to different

steps in layer deposition process hinder observing the peaks of interest and therefore such spectra were not illustrated here. Instead, another excitation wavelength allows obtaining better spectra. A representative such SERS spectrum is shown in Figure 6. The latter spectrum is dominated by two peaks with high surface enhancement, at ca. 1000 and 3080  $\text{cm}^{-1}$ ; that is why it was almost impossible to perform a good deconvolution for the peaks of interest.

On the basis of the previously proposed band assignments in RS and surface enhanced Raman spectra of related compounds (see Refs. [47–49]), one may deduce the assignment of the most bands in the spectra of deposited thiol layer in our samples. The bands at 2800–3000  $\text{cm}^{-1}$  should be assigned to the  $\nu(\text{C-H})$  vibrations [48]. In our SERS spectrum as well as in the spectra of many compounds containing an aromatic ring, the band due to the “breathing vibration” of the ring (at ca. 1000  $\text{cm}^{-1}$ ) is often very strong [49]. The same seems to be the case of the CH stretching peaks of the aromatic part. Both peaks probably appear from the polystyrene substrate.

An analysis of monolayer spectra on the basis of SERS selection rules [50–52] would conclusively establish a near-perpendicular molecular geometry. Unfortunately, the C-S stretching peak located at around 700  $\text{cm}^{-1}$  cannot be distinguished from the noise in our samples and no normalization of the experimental data to an internal standard could be done to avoid differences among the different spectra obtained [53].

It is well known that SERS spectra of alkanethiol SAMs on top of a silver surface possess some peculiar characteristics different from the bulk which testify to both the chemisorption and self-assembling into an ordered molecular array [54]. Indeed, the most valuable signals due to  $\text{CH}_2/\text{CH}_3$  groups are given in the region of CH stretching between 2800 and 3100  $\text{cm}^{-1}$ . Chemisorption of the alkanethiols can be generally observed because of the lack of the SH stretching peak at 2575  $\text{cm}^{-1}$ ; this seems to be the case of our samples too. Moreover, to be sure that the chemisorption really took place, we prepared samples having higher concentration of the species. No peak appeared indeed at the mentioned position.

Table 4. Assignment of some Raman peaks in the alkanethiol (position in  $\text{cm}^{-1}$ ).

Vibration mode	Position
$\text{CH}_2$ symmetric stretch	2850
$\text{CH}_2$ symmetric stretch	2861
$\text{CH}_3$ symmetric stretch	2875
$\text{CH}_2$ asymmetric stretch	2900
$\text{CH}_3$ symmetric stretch FR*	2935
$\text{CH}_3$ asymmetric stretch	2965

\* FR denotes Fermi resonance.

In Table 4 we give the vibrational frequencies (and their assignment according to literature [53]) which were involved in the region plotted in the inset of Fig. 5.

### 3.2. Orientation of 5CB molecules by the functionalized gold layers

The orientation of liquid crystal produced by different layers was analyzed between crossed polarizers in a parallel light beam (orthoscopic technique) or in a convergent light beam (conoscopic technique). The former technique is suitable to put in evidence the uniformity of the orientation of the liquid crystal molecules inside the cells. The latter technique allows to observe the tilted textures and to assign the tilt sense like the A, H, B in the Fig. 1.

The present images were taken for the cells situated on the microscope stage with the orientation as in Figure 1. The polarizer is oriented along the projection of the evaporation direction onto the glass plate.

The conoscopic technique was already used in the literature to follow up the effect of the organic layers on the LC alignment (e.g. see [55,56]).

In the conoscopic technique applied in the present work, a tilted orientation direction is given by the position (central or more or less shifted) of the symmetry center of the observed interference figure. In the case of a tangential orientation, the orientation direction might be in the evaporation plane or perpendicular on it. To determine this orientation direction asks for properly using a compensator. In our case, one has to take into consideration that 5CB has a positive optical anisotropy.

The LC orientation in the cells with nanostructured gold layer (without SAM layer) deposited under our experimental conditions was previously analyzed in ref. [12,16]. It was shown that the orientation is in the incidence plan of the gold vapors but with a tilt angle depending on the incidence angle and on the thickness of the gold layer, being either perfect homeotropic (H direction in Figure 1) or with an orientation in incidence plane between a weak tilt type A or strong tilt type B (A and B directions in Figure 1). Our initial observations were made within a few min of filling the optical cells with liquid crystal.

Functionalization of nanostructured gold layer by hexadecanethiol SAMs changes the orientation of the LC molecules, depending on the thicknesses and/or deposition angles. Thus, in the cells with  $\theta = 80^\circ$  deposition angle, without SAM (see Figure 7a), the orientation was in the incidence plane, tilted in the evaporation direction as shown by B direction in Figure 1. The SAM layer added on this gold layer leads to an orientation in the incidence plane, tilted in the direction opposite to the evaporation one as shown by A direction in Fig. 1.

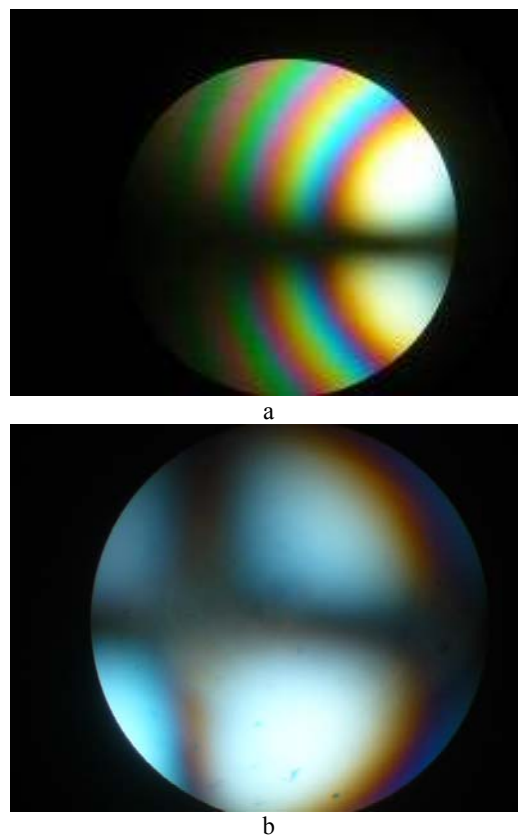
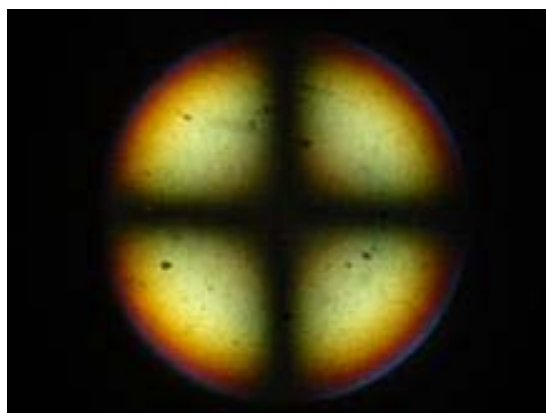
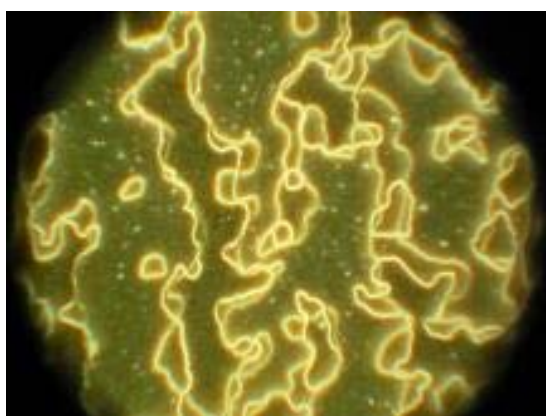


Fig. 7. Conoscopic images (between crossed polarizers) (viewed in colors in the online issue) of 5CB orientation in the cells with gold layer deposited at  $80^\circ$  without and with SAM overlayer: (a) cell with P(2) plates; (b) cell with C16SH-P(2) plates.

Among the cell studied, the most important change has been produced for deposition of gold layer at  $60^\circ$  and thickness of 20 nm. When the cells without SAM were filled with liquid crystal, the orientation was homeotropic (Figure 8a). In the cells with SAM containing plates the orientation is tangential in the direction perpendicular to the evaporation plane; the anchoring is weak. Because the cells with such P orientation lead to black conoscopic images, in Figure 8b the orientation is shown orthoscopic (in parallel light beam) only. The presence of orientation defects and discontinuities in the optical texture shows a weak anchoring strength. It has been mentioned in the literature (cited in [57]) that planar anchoring of 5CB is observed on a variety of closely packed SAMs on gold that have different degrees of molecular tilt ( $0^\circ$  to  $30^\circ$ ).



(a)



(b)

Fig. 8. (a) Conoscopic image (between crossed polarizers) of 5CB orientation in the cell with P(6) plates. (b) Orthoscopic image (between crossed polarizers) of the LC orientation in the cell with SAM functionalized P(6) plates. (The images are viewed in

colors in the online issue).

#### 4. Conclusions

Self-assembling of hexadecanethiol monolayers onto nanostructured gold layers deposited at small incidence angle upon polystyrene layers was achieved first time.

We found that the glass plates based on gold deposition onto an intermediate PS layer do not peel under overnight immersing in ethanol solution of hexadecanethiol.

The thiol and gold layers were characterized by complementary methods. The thickness of the thiol layer was deduced from SE measurements to be ca. 1 nm, meaning less than the length of the molecule; it was then inferred that the molecule is tilted onto gold, as expected from the behavior of other self assembled monolayers (SAMs) obtained under similar conditions. In fact, the hexadecanethiol molecule is bonded to the gold atoms as thiolate species, as shown by the XPS and Raman spectroscopy measurements.

The ellipsometric thickness of our SAMs indicates a SAM thicker on sample C16SH-P(4) than on C16SH-P(3) in agreement with the XPS measurements.

The alignment of a nematic liquid crystal was used to probe the structure of organic surface. The cells having both plates deposited with the hexadecanethiol SAMs are still uniform, despite the multilayer structure of the substrate on the glass plates.

#### Acknowledgements

The authors thank the Romanian Ministry of Education and Research for financial support by the PNII Project VIRNANO/2007. Valuable discussions with Dr. C. Logofatu are highly appreciated.

#### References

- [1] R. G. Nuzzo, D. L. Allara, J. Amer. Chem. Soc., **105**, 4481 (1983).
- [2] C. D. Bain, E. B. Troughton, Y.-T. Tao, J. Evall, G. M. Whitesides, R. G. Nuzzo, J. Amer. Chem. Soc., **111**, 321 (1989).
- [3] M. D. Porter, T. B. Bright, D. L. Allara, C. E. D. Chidsey, J. Amer. Chem. Soc., **109**, 3559 (1987).
- [4] G. M. Whitesides, P. E. Laibinis, Langmuir, **6**, 87 (1990).
- [5] V. K. Gupta, N. L. Abbott, Langmuir **12**, 2587 (1996).
- [6] B. H. Clare, O. Guzman, J. J. de Pablo, N. L. Abbott, Langmuir **22**, 4654 (2006).
- [7] V. K. Gupta, J. J. Skaife, T. B. Dubrovsky, N. L. Abbott, Science, **279**, 2077 (1998).
- [8] J. J. Skaife, J. M. Brake, N. L. Abbott, Langmuir, **17**, 5448 (2001).
- [9] Y.-Y. Luk, M. L. Tingey, D. J. Hall, B. A. Israel, C. J. Murphy, P. J. Bertics, N. L. Abbott, Langmuir, **19**, 1671 (2003).
- [10] L. A. Tercero Espinoza, K. R. Schumann, Y.-Y. Luk, B. A. Israel, N. L. Abbott, Langmuir, **20**, 2375 (2004).
- [11] J. J. Skaife, N. L. Abbott, Langmuir **17**, 5595 (2001).
- [12] T. Beica, S. Frunza, I. Zgura, L. Frunza, C. Cotarlan, C. Negriila, A. M. Vlaicu, C. N. Zaharia, J. Optoelectron. Adv. Mater., Submitted (2009). Part I.
- [13] Y. Gu, N. L. Abbott, Phys. Rev. Lett. **85**, 4719 (2000).
- [14] R. R. Shah, N. L. Abbott, J. Phys. Chem. B **105**, 4936 (2001).
- [15] N. L. Abbott, J. J. Skaife, US Patent 6288392 (2001).
- [16] I. Zgura, T. Beica, S. Frunza, O. Rasoga, A. Galca, L. Frunza, A. Moldovan, M. Dinescu, C. Zaharia, J. Optoelectron. Adv. Mater. Submitted (2009) Part II.
- [17] P. N. Sanda, D. B. Dove, H. L. Ong, S. A. Janssen, R. Hoffmann, Phys. Rev. A, **39**, 2653 (1989).

- [18] D. N. Stoenescu, S. Frunza, V. Roques, J. Ferenc, J. P. Traverse, *Cryst. Res. Technol.*, **31**, 1095 (1996).
- [19] S. Frunza, G. Grigoriu, A. Grigoriu, C. Luca, L. Frunza, R. Moldovan, D. N. Stoenescu, *Cryst. Res. Technol.*, **32**, 989 (1997).
- [20] C. C. Negrila, C. Logofatu, R. V. Ghita, C. Cotirlan, F. Ungureanu, A. S. Manea, M. F. Lazarescu, *J. Crystal Growth*, **310**, 1576 (2008).
- [21] Z. Hou, N. L. Abbott, P. Stroeve, *Langmuir*, **14**, 3287 (1998).
- [22] M. A. Daza Millone, H. Hamoudi, L. Rodríguez, A. Rubert, G. A. Benítez, M. E. Vela, R. C. Salvarezza, J. E. Gayone, E. A. Sanchez, O. Grizzi, C. Dablemont, V. A. Esaulov, *Langmuir*, **25**, 12945 (2009).
- [23] P. Harder, M. Grunze, R. Dahint, G. M. Whitesides, P. E. Laibinis, *J. Phys. Chem. B*, **102**, 426 (1998).
- [24] C. Pale-Grosdemange, E. S. Simon, K. L. Prime, G. M. Whitesides, *J. Am. Chem. Soc.*, **113**, 12 (1991).
- [25] N.-P. Huang, R. Michel, J. Voros, M. Textor, R. Hofer, A. Rossi, D. L. Elbert, J. A. Hubbell, N. D. Spencer, *Langmuir*, **17**, 489 (2001).
- [26] Z. Hou, N. L. Abbott, P. Stroeve, *Langmuir* **14**, 3287 (1998).
- [27] H.-L. Zhang, S. D. Evans, K. Critchley, H. Fukushima, T. Tamaki, F. Fournier, W. Zheng, S. Carrez, H. Dubost, B. Bourguignon, *J. Chem. Phys.* **122**, 224707 (2005).
- [28] P. E. Laibinis, G. M. Whitesides, D. L. Allara, Y. T. Tao, A. N. Parikh, R. G. Nuzzo, *J. Am. Chem. Soc.*, **113**, 7152 (1991).
- [29] C. D. Bain, H. A. Biebuyck, G. M. Whitesides, *Langmuir*, **5**, 723 (1989).
- [30] W. R. Salaneck, N. O. Lipari, A. Paton, R. Zallen, K. S. Liang, *Phys. Rev. B*, **12**, 1493 (1975).
- [31] D. G. Castner, K. Hinds, D. W. Grainger, *Langmuir*, **12**, 5083 (1996).
- [32] J. Heeg, U. Schubert, F. Küchenmeister, *Fresenius J. Anal. Chem.*, **365**, 272 (1999).
- [33] T. M. Willey, A. L. Vance, T. van Buuren, C. Bostedt, L. J. Terminello, C. S. Fadley, *Surface Sci.* **576**, 188-196 (2005).
- [34] J. Leiro, E. Minni, E. Suoninen, *J. Phys. F: Metal Physics* **13**, 215 (1983).
- [35] N. Aldea, P. Marginean, V. Rednic, S. Pintea, B. Barz, A. Gluhoi, B. E. Nieuwenhuys, X. Yaning, F. Aldea, M. Neumann, *Digest J. Nanomater. Biostruct.* **1**, 71 (2006).
- [36] J. Cazaux, *J. Electron Spectrosc. Relat. Phenom.* (2009), doi:10.1016/j.elspec.2009.03.007.
- [37] C. D. Wagner, Riggs, W. M.; Davis, L. E.; Moulder, J. F. *Handbook of X-ray Photoelectron Spectroscopy*; Muilenberg, G. E., Ed.; Perkin-Elmer Corporation: Eden Prairie, MN, 1979.
- [38] B. Dordi, H. Schonherr, G. J. Vancso, *Langmuir*, **19**, 5780 (2003).
- [39] R. G. Nuzzo, D. L. Allara, *J. Am. Chem. Soc.*, **105**, 4481 (1983).
- [40] C. D. Bain, E. B. Troughton, Y.-T. Tao, J. Evall, G. M. Whitesides, R. G. Nuzzo, *J. Am. Chem. Soc.*, **111**, 321 (1989).
- [41] M. D. Porter, T. B. Bright, D. L. Allara, C. E. D. Chidsey, *J. Am. Chem. Soc.*, **109**, 3559 (1987).
- [42] R. M. A. Azzam, N. M. Bashara, *Ellipsometry and Polarized Light*, North Holland, Amsterdam, 1977.
- [43] J. Shi, B. Hong, A. N. Parikh, R. W. Collins, D. L. Allara, *Chem. Phys. Lett.*, **246**, 90 (1995).
- [44] O. Cavalleri, M. Prato, A. Chincarini, R. Rolandi, M. Canepa, A. Gliozzi, M. Alloisio, L. Lavagnino, C. Cuniberti, C. Dell'Erba, G. Dellepiane, *Appl. Surf. Sci.*, **246**, 403 (2005).
- [45] R. R. Shah, D. M. Heinrichs, N. L. Abbott, *Colloids and Surfaces, A: Physicochemical and Engineering Aspects*, **174**, 197 (2000).
- [46] B. J. Kennedy, S. Spaeth,† M. Dickey, K. T. Carron, *J. Phys. Chem. B*, **103**, 3640 (1999).
- [47] A. Kudelski, *Vibr. Spectrosc.*, **46**, 34 (2008).
- [48] E. Podstawka, Y. Ozaki, L. M. Proniewicz, *Appl. Spectrosc.*, **58**, 1147 (2004).
- [49] B. Pettinger, H. Wetzel, *Ber. Bunsenges. Phys. Chem.*, **85**, 473 (1981).
- [50] M. Moskovits, J. S. Suh, *J. Phys. Chem.* **88**, 5526 (1984); M. Moskovits, J. S. Suh, *J. Phys. Chem.* **92**, 6327 (1988).
- [51] J. A. Creighton, *Surf. Sci.* **124**, 204 (1983).
- [52] N. Sandhyarani, G. Skanth, S. Berchmans, V. Yegnaraman, T. Pradeep, *J. Colloid Interface Sci.* **209**, 154 (1999).
- [53] G. Compagnini, C. Galati, S. Pignataro, *Phys. Chem. Chem. Phys.*, **1**, 2351 (1999).
- [54] M. K. Bryant, J. E. Pemberton, *J. Am. Chem. Soc.*, **113**, 3629 (1991).
- [55] V. K. Gupta, N. L. Abbott, *Langmuir*, **15**, 7213 (1999).
- [56] J. J. Skaife, N. L. Abbott, *Langmuir*, **16**, 3529 (2000).
- [57] W. J. Miller, N. L. Abbott, *Langmuir*, **13**, 7106 (1997).

\*Corresponding author: lfrunza@infim.ro